



Research Article

Numerical investigation of improved metal foam heat sink with $\text{Fe}_3\text{O}_4\text{-H}_2\text{O}$ nanofluid

T. BOUACIDA^{1,*}, R. BESSAÏH¹

¹LEAP Laboratory, Department of Mechanical Engineering, University of Mentouri Brothers-Constantine 1, 25017, Algeria

ARTICLE INFO

Article history

Received: 23 August 2023

Revised: 08 February 2024

Accepted: 14 February 2024

Keywords:

Electronic Cooling; Forced Convection; Heat Sink; Two-Phase Eulerian Model; Porous Media

ABSTRACT

The reliability and efficiency of electronic systems can be improved by removing their high thermal flux. Integrating porous media and nanofluids as working fluid within a heat sink (HS) is an effective strategy to dissipate the heat of electronic devices. To cool a CPU, a three-dimensional numerical simulation is carried out to investigate the characteristics of $\text{Fe}_3\text{O}_4\text{-H}_2\text{O}$ nanofluid flow, heat transfer, and entropy production in the proposed heat sink equipped with enhanced metal foam. The two-phase Eulerian model is implemented in Ansys Fluent software to predict the behavior of the turbulence flow of nanofluid. The simulation results are validated with experimental and numerical existing data, good agreement is achieved. The impact of pore permeability ($10^{-4} \leq \text{Da} \leq 10^{-1}$), nanoparticle diameter ($10\text{nm} \leq \text{dn} \leq 50\text{nm}$), nanoparticle concentration ($0.1\% \leq \varphi \leq 0.5\%$), and flow velocity ($2600 \leq \text{Re} \leq 3800$) on heat exchange and entropy generation/production are carried out. The results showed that the application of reinforced foam enhances the average Nusselt number by 5.79% compared to aluminum foam and reduces thermal entropy generation/production by 47.58% at $\text{Re} = 2600$. Moreover, the performance evaluation criteria (PEC) increase by 56% when the pore permeability and flow velocity are raised.

Cite this article as: Bouacida T, Bessaïh R. Numerical investigation of improved metal foam heat sink with $\text{Fe}_3\text{O}_4\text{-H}_2\text{O}$ nanofluid. J Ther Eng 2025;11(1):62–78.

INTRODUCTION

Microelectronic components have become indispensable in most fields, particularly media, communications, and security. As the demand for information technology grows, saving time and effort has become crucial. However, heat generation from electronic devices is a major issue that researchers and scientists are trying to minimize, as it is the main cause of their short lifespan and damage.

Nanofluids have attracted researchers' attention as one of the solutions, as they are considered the best alternative to air in terms of heat exchange and cooling efficiency [1, 2], as confirmed by several experimental studies [3]. Porous media and heat sinks are also technologies that improve heat transfer and have attracted prominent researchers [4, 5]. Dong et al. [6] studied a radial HS with triangular fins installed on a concentric cylinder and found that it reduces thermal resistance and mass compared to a reference heat

*Corresponding author.

*E-mail address: touba.bouacida@gmail.com

This paper was recommended for publication in revised form by Editor-in-Chief Ahmet Selim Dalkılıç



sink. They proved that the mass and resistance of HS decreased by 10-13% compared with reference radial HS.

Wu et al. [7] performed a numerical study on the impact of various flow and permeability characteristics on HS efficiency filled with metal foams at different arrangements to evaluate heat sink performance. E. Moghadam and J. Moghadam [8] simulated the turbulent flow of Alumina-nf in corrugated heat exchangers and found that adding 4% Al_2O_3 causes an irreversibility increase of at most 5%. To the same aim, He et al. [9] conducted a numerical study of the geometrical parameters of ribbed pin micro-dissipators. They found that the average Nusselt number reached 44.3 at $\text{Re}=1342$.

Ming Jeng et al. [10] experimentally conducted square-finned HS cooling using a passage divider by forced water convection. Their results showed that Nu's global improvement is 65% compared to HS without a passage divider and packed brass beads. Khan et al. [11] studied a hybrid nanofluid's mixed axial heat flow problem through a vertical cylinder filled with irradiated porous foam and a non-uniform heat source/dissipator. Ahmadian-Elmi et al. [12] conducted the effect of a pulsed heat pipe on the geometrical parameters of a micro-channel heat sink (MCHS) to reduce the temperature of electronic components. Yao et al. [13] examined heat exchanger and irreversibility of a non-Newtonian nf in a silicon MCHS. They found that adding nanoparticle concentration with increased sliding length reduced the total entropy generation by 2.55%. Kavitha et al. [14] performed a computational analysis of five-channel HS using $\text{Al}_2\text{O}_3/\text{H}_2\text{O}$ nf and distilled water as cooling fluids. The heat transfer coefficient increased by 51% when using nf compared to distilled water.

The impact of a jet with a magnetic field can also yield good results in heat exchanger and entropy production. Tilehnoee and Barrio [15] analyzed heat exchanger and entropy generation on a surface heated by a slit jet subjected to a uniform magnetic field and cooled by different nanofluids. They demonstrated that magnetic field applications could effectively reduce entropy generation. Wang et al. [16] evaluated an Oldroyd-B fluid's heat and mass transfer on a surface exposed to thermal radiation and a magnetic field. Furthermore, Tilehnoee et al. [17] considered a heated square container with 16 and 64 cylindrical solid blocks under a magnetic field to evaluate heat transfer and entropy generation. Their results showed that Rayleigh and Hartmann's numbers raised average Nusselt number and entropy production.

Entropy generation effects on the flow of three different hybrids in the Carreau-ternary with a magnetic field applied to a 2D stretching area were studied by Ramzan et al. [18]. Magnetohydrodynamics (MHD) improved convection in a metal HS filled with aluminum foam, and nf was studied by Izadi et al. [19]. Using a high magnetic field with porous foam improved impingement cooling heat transfer. Mass and heat transfer effects on the bio-convective magnetohydrodynamic peristaltic transport of Powell-Eyring nf

through a curved channel with a magnetic field were studied by Iqbal et al. [20]. Flow and heat exchanger characteristics of nf jet impaction on an MCHS with corrugated bottom were proposed and numerically studied by Cheng et al. [21]. Based on their findings, when the resistance of MCHS is optimized, the pumping power is decreased.

Kushawaha et al. [22] examined a numerical study of 2D natural convection of $\text{Fe}_3\text{O}_4\text{-H}_2\text{O}$ nf and $\text{Cu-H}_2\text{O}$ non-magnetic nf inside a concentrated and exo-concentrated heated enclosure. They concluded that, at a higher value of nanoparticle concentration (ϕ %), the heat transfer reduced by 10% for $\text{Fe}_3\text{O}_4\text{-H}_2\text{O}$ and 12% for $\text{Cu-H}_2\text{O}$ nf. Reddy et al. [23] studied porosity effects in the presence of radiation and viscous dissipation on heat and mass transfer by 2D unsteady MHD mixed convection.

A two-phase mixing model was employed by Baghratz et al. [24] to study the role of np sedimentation on the parameters of natural convection heat exchanger within a porous channel filled with $\text{Al}_2\text{O}_3\text{-H}_2\text{O}$ nf through time. Their results showed that the formation of np deposition layers reduced Nu number. Five rib configurations in the interrupted microchambers of MCHSs were analyzed by Chai and Wang[25] to identify their thermal-hydraulic performances. Several studies have been investigated to achieve the same goal [26-38].

Farrukh et al. [39] studied the influence of viscous dissipation on plate channel temperature used for electronic cooling. The floating convection and heat dissipation of a saturated hybrid nf in inclined porous pipe were studied by Reddy et al. [40] using the Darcy-Brinkman-Forchheimer model. They were raising Darcy's number and improved heat dissipation. Zhang et al. [41] applied the topological optimization method to study the geometrical design of 2D MCHS that cools by $\text{Al}_2\text{O}_3/\text{H}_2\text{O}$ nf. Yang and Cao [42] proposed a multi-objective optimization of hybrid MCHS that combines the manifold concept with secondary oblique channels.

One solution proposed to enhance heat dissipation in electronic components is using phase change materials. Krishnan et al. [43] experimentally and numerically assessed the influence of Neopentyl glycol (NPG) on phase change material (PCM) HS operation with heat pipe-assisted solid-solid phase transition. They found that integrating heat pipes with a PCM-assisted HS significantly improved efficiency. Mirshekar et al. [44] performed experimental research on the impact of application PCMs embedded in an open-cell Cu-foam in an HS during the heating and cooling process on different samples. Rahman et al. [45] proposed an experimental study on a nickel foam HS embedded with PCM. They noted that the base temperature of HS decreased by 23% when using nickel foam and PCM.

The literature mentioned above has highlighted various methods that are currently used to dissipate heat from microelectronic devices to preserve their efficiency and age for much longer. The study's main objective is to cool

Table 1. Physical properties of base metal foam studied

Properties	Al-foam [46]	Cu-foam	Al-Cu1 foam	Al-Cu2 foam	Al-Cu3 foam
k (W/m.K)	218	401	254.6	272.9	291.2
ρ (kg/m ³)	2719	8960	3967.2	4591.3	5215.4
Cp (J/kg.K)	871	390	774.8	726.7	678.6

a CPU using a proposed HS with a metal foam and nano-fluid. The key points raised in this study are set out below:

- The heat sink was created with dimensions adapted to Core i9 processor sizes, which have not yet been considered.
- The idea proposed is an improved foam made with a combination of variable ratios of aluminum and copper in place of currently used metallic foams aluminum or copper to study their effectiveness in heat transfer and entropy generation.
- Improved porous foam is placed within the heat sink in opposite directions, with the two porous fins facing each other.
- Turbulence flow of nanofluid is used instead of water to enhance heat transfer.

Various parameters that affect heat transfer and entropy generation, such as pore permeability ($10^{-4} \leq Da \leq 10^{-1}$), nanoparticle diameter ($10\text{nm} \leq d_n \leq 50\text{nm}$), nanoparticle concentration ($0.1\% \leq \phi \leq 0.5\%$), and flow velocity ($2600 \leq Re \leq 3800$) are taken into account. Using a two-phase Eulerian model to predict the behavior of $\text{Fe}_3\text{O}_4/\text{H}_2\text{O}$ nf is a suitable approach, giving insight into the complex interactions between nf and porous foam. The optimal ratio of the aluminum-copper mixture in the porous foam is determined, which can potentially improve the performance of HS used in microelectronic devices. Overall, the study may contribute to developing more efficient cooling systems for microelectronic components.

PROBLEM DESCRIPTION AND GOVERNING EQUATIONS

This study aims to simulate the proposed design of a heat sink to cool the i9 CPU with metal foam containing aluminum and copper in different proportions to achieve the most efficient foam. The properties of the base metal foam used are shown in Table 1, with a constant metal foam porosity $\varepsilon = 0.8$. The physical depiction of the studied area is illustrated in Figure 1. $\text{Fe}_3\text{O}_4\text{-H}_2\text{O}$ nf is used as a coolant, the effect of nanoparticles diameter ($10\text{nm} \leq d_n \leq 50\text{nm}$) and their concentrations ($0.1\% \leq \phi \leq 0.5\%$) on heat transfer and entropy generation are studied. Nanofluid characteristics are presented in Tab.2. A turbulent nf flow ($2600 \leq Re \leq 3800$) is applied to the porous medium, entered at $T = 293.16\text{ K}$ to evacuate the heat flux distributed on the bottom surface of HS (220 kW/m^2).

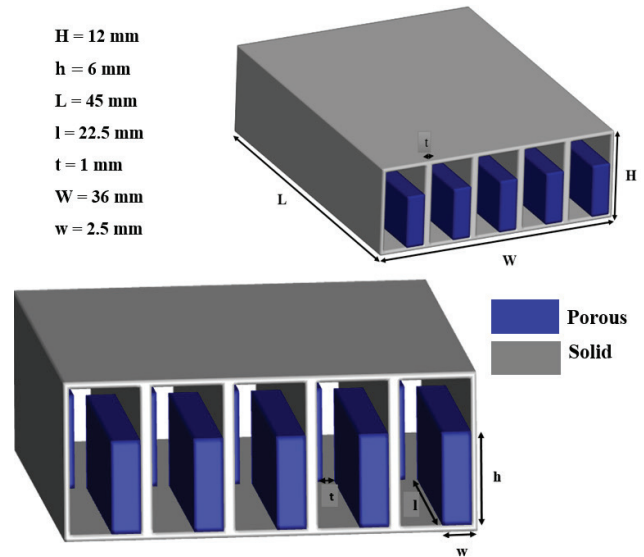


Figure 1. Schematic of the heat sink, including porous fins of Al-Cu3 foam.

Nanofluid flow is assumed to be steady-state, incompressible, 3D, with constant thermophysical properties and two-phase (mixing and Eulerian) conditions throughout the studied field to model the computational domain and simulation. The radiative mode of heat transfer between the two phases is negligible. Fe_3O_4 nanoparticles and H_2O constitute two interpenetrating liquid phases. Moreover, porous foam is homogeneous, isotropic, and in thermal equilibrium with nf, with a constant porosity.

Eulerian Multiphase Method

According to the Eulerian model, the governing equations based on the above hypotheses are:

The continuity equations of the second phase are defined as follows [47]:

$$\nabla \cdot (\varphi_p \rho_p V_p) = 0 \quad (1)$$

$$\nabla \cdot (\varphi_l \rho_l V_l) = 0 \quad (2)$$

The momentum equations for the two phases are as follows [47]:

$$\nabla \cdot (\varphi_p \rho_p V_p V_p) = -\varphi_p \nabla P + \nabla \cdot \overline{T_p} + F_{pl} \quad (3)$$

$$\nabla \cdot (\varphi_1 \rho_1 V_1 V_1) = -\varphi_1 \nabla P + \nabla \cdot \bar{T}_1 + F_{lp} \quad (4)$$

The F_{pl} and F_{lp} identify the forces interacting between the two phases, V_p and V_l represent the velocity of solid and liquid phases, respectively.

The energy equation of the Eulerian phases is more approximate by [47]:

$$\nabla \cdot (\varphi_p \rho_p h_p V_p) = \bar{T}_p : \nabla V_p - \nabla \cdot k_p \nabla T + q_{pl} \quad (5)$$

$$\nabla \cdot (\varphi_l \rho_l h_l V_l) = \bar{T}_l : \nabla V_l - \nabla \cdot k_l \nabla T + q_{lp} \quad (6)$$

Where h_p and h_l are specific enthalpies of solid and liquid phases, respectively. The q_{pl} and q_{lp} identify the rate of heat exchanger between solid and liquid phases. \bar{T}_p and \bar{T}_l identify the stress-strain tensor of solid and liquid phases.

k-ε Turbulence Model

The k-ε standard model is a one-based on transport equations for kinetic energy of turbulence (k) and its rate of dissipation (ε) [51], which are found in the equations below:

$$\frac{\partial}{\partial t} (\rho k) + \frac{\partial}{\partial x_i} (\rho k u_i) = \frac{\partial}{\partial x_j} \left[\left(\mu + \frac{\mu_t}{\sigma_k} \right) \frac{\partial k}{\partial x_j} \right] + G_k + G_b - \rho \varepsilon - Y_m + S_k \quad (7)$$

$$\frac{\partial}{\partial t} (\rho \varepsilon) + \frac{\partial}{\partial x_i} (\rho \varepsilon u_i) = \frac{\partial}{\partial x_j} \left[\left(\mu + \frac{\mu_t}{\sigma_\varepsilon} \right) \frac{\partial \varepsilon}{\partial x_j} \right] + C_{1\varepsilon} \frac{\varepsilon}{k} (G_k + C_{3\varepsilon} G_b) - C_{2\varepsilon} \rho \frac{\varepsilon^2}{k} + S_\varepsilon \quad (8)$$

G_k and G_b represent the kinetic energy production of turbulence due to velocity gradients and buoyancy, respectively. Y_m is the fluctuating dilatation contribution in compressible turbulence to the global dissipation rate. $C_{1\varepsilon}$, $C_{2\varepsilon}$, and $C_{3\varepsilon}$ are constants which $C_{1\varepsilon} = 1.44$, $C_{2\varepsilon} = 1.92$, $C_{3\varepsilon} = 1.63$ [51].

σ_k and σ_ε are the turbulence Prandtl numbers for k and ε ($\sigma_k = 1$, $\sigma_\varepsilon = 1.3$) [51], S_k and S_ε are source terms.

Turbulence viscosity μ_t is determined by combining k and ε in the following way [51]:

$$\mu_t = \rho C_\mu \frac{k^2}{\varepsilon} \quad (9)$$

C_μ is a constant equal to 0.09.

Thermophysical Properties of Nanofluid

The physical characteristics of Fe_3O_4 - H_2O nf are presented in Table 2. The density (ρ_{nf}), dynamic viscosity (μ_{nf}), and specific heat ($C_{p,nf}$) of nf are calculated by the following equations [48]:

$$\rho_{nf} = (1 - \varphi) \rho_l + \varphi \rho_p \quad (10)$$

$$\mu_{nf} = \frac{\mu_l}{(1 - \varphi)^{2.5}} \quad (11)$$

$$C_{p,nf} = (1 - \varphi) C_{p,l} + \varphi C_{p,p} \quad (12)$$

The nanofluid thermal conductivity (k_{nf}) is calculated by [49]:

$$k_{nf} = k_l \left[\frac{k_l + 2k_p + 2\varphi(k_p - k_l)}{k_p + 2k_l - \varphi(k_p - k_l)} \right] \quad (13)$$

Data Reduction

The average Nusselt number (Nu_{avg}) is calculated by [9]:

$$Nu = \frac{k_{nf}}{k_l} \left(\frac{\partial T}{\partial x} \times \frac{D_h}{T_{in}} \right) \quad (14)$$

$$Nu_{avg} = \frac{1}{A} \int Nu \, dA \quad (15)$$

The Reynolds number [3]

$$Re = \frac{\rho_l V D_h}{\mu_l} \quad (16)$$

Hydraulic diameter is defined as follows [3]:

$$D_h = \frac{4A_f}{P} = 2 \frac{ab}{a+b} \quad (17)$$

The permeability of nf through porous media can be indicated by Darcy's number. Defined by [3]:

$$Da = \frac{K}{D_h^2} \quad (18)$$

The equation below was employed to compute pressure drop in the working domain [9]:

$$\Delta P = P_{in} - P_{out} \quad (19)$$

Table 2. Physical properties of Fe_3O_4 - H_2O nanofluid [48]

Physical properties	ρ (kg/m ³)	C_p (J/kg.K)	k (W/m.K)	μ (Pa.s)
Water H_2O	998.1	4179	0.613	0.0013004
Fe_3O_4 nanoparticle	5180	670	80	/

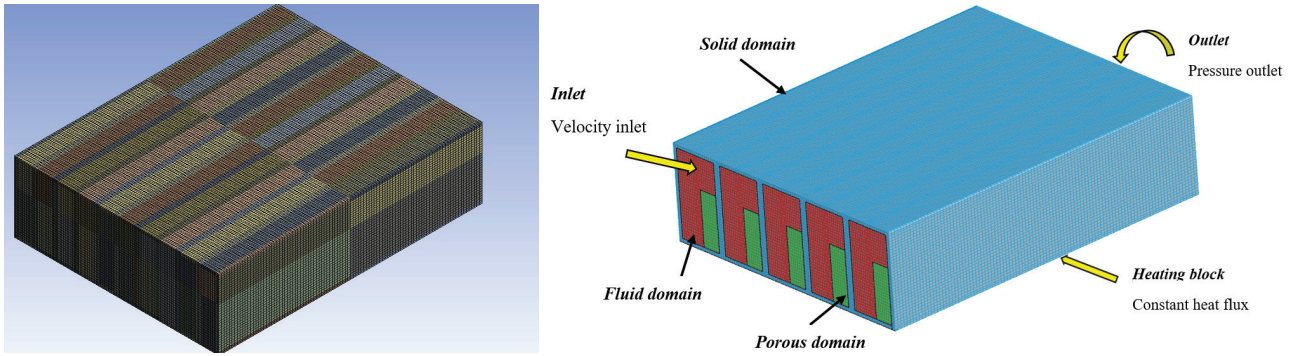


Figure 2. Mech topology and boundary conditions.

Eqs estimate Performance Evaluation Criterion (PEC) and friction factor (f) are [47]:

$$PEC = \frac{Nu_{nf}}{\frac{\Delta P_{nf}}{\Delta P_1}} \quad (20)$$

$$f = \frac{\Delta P \cdot D_h}{2 \times (L \times \rho_{nf} \times V^2)} \quad (21)$$

Entropy Production

The total entropy generation (S_g) of the system constitutes thermal (S_h), viscous (S_f), and porous (S_p) entropy components [47]

$$S_h''' = \frac{k_{nf}}{T^2} \left[\left(\frac{\partial T}{\partial x} \right)^2 + \left(\frac{\partial T}{\partial y} \right)^2 + \left(\frac{\partial T}{\partial z} \right)^2 \right] \quad (22)$$

$$S_f''' = \frac{\mu_{nf}}{T} \left\{ 2 \left[\left(\frac{\partial u}{\partial x} \right)^2 + \left(\frac{\partial v}{\partial y} \right)^2 + \left(\frac{\partial w}{\partial z} \right)^2 \right] + \left(\frac{\partial v}{\partial x} + \frac{\partial u}{\partial y} \right)^2 + \left(\frac{\partial w}{\partial y} + \frac{\partial v}{\partial z} \right)^2 + \left(\frac{\partial u}{\partial z} + \frac{\partial w}{\partial x} \right)^2 \right\} \quad (23)$$

$$S_p''' = \frac{\mu_{nf}}{T \cdot K} (u^2 + v^2 + w^2) \quad (24)$$

K represent the permeability of metal foam.

$$S_g = S_h + S_f + S_p \quad (25)$$

The system's global entropy is the integral of total entropy over the computation domain [47]

$$S_g = \int S_h''' dv + \int S_f''' dv + \int S_p''' dv \quad (26)$$

Boundary Conditions

Flow problems can be numerically solved by setting the correct boundary conditions (Fig. 2), as follows:

- Inlet boundary: $u = 0$, $v = 0$, $w = w_{in}$ (uniform velocity), and $T = T_{in} = 293.15K$.
- Outlet boundary: $P = P_{out}$ (Atmospheric).
- Walls boundary: At no-slip condition $u = v = w = 0$.
- Heat source: $q'' = 220 \text{ kW/m}^2$.

Numerical Approach, Grid Independence, and Validation

The ANSYS-Fluent software is used in the numerical study [51]. A simple algorithm based on the finite volume method (FVM) is utilized to discretize and solve the partial differential equations (1-8). The second-order upwind schema is adopted to realize the coupling of velocity and pressure terms in momentums and energy equations. Flow and temperature fields are not affected by thermal radiation. $k-\epsilon$ standard model is selected to investigate the turbulence effect of nf flow in HS. To maintain good accuracy of results, the residual's convergence error is between 10^{-6} and 10^{-7} . Constant velocity inlet, atmospheric pressure outlet, and constant heat flux q'' boundary conditions (Fig. 2), no-slip boundary conditions for solid-fluid, solid-porous, and fluid-porous interfaces are applied to the computational domain.

A structured mech of hexagonal elements was established for this study. Figure 3 shows the central processing unit's (CPU's) contact surface temperature variations on five meshes (288000–480000 components) to demonstrate the grid's independence. It can be seen that grid 4 (432000 elements) is well with grid 3 (388800 elements). The acquired error between them is below 0.007% in temperature surface. This indicates that the quality of grid 4 gives accurate results, so it is adopted in the simulation of this study, shown in Figure 2.

This study compares the results of the new computational model to Alhajaj et al. [50] and Ambreen et al. [47]. For validation, a five-channel HS with a length of 45 mm, width of 6 mm, and height of 12 mm was tested. The HS bottom is filled with the opposite porous foam (properties are illustrated in Table 1) with dimensions $l \times w \times h$ (Fig. 1). A mono-phase model and laminar forced convection of water are applied to metal foam ($\epsilon = 0.9$).

Figure 4 shows Nusselt's average number (Nu_{avg}) on the different flow rates (0.1, 0.15, 0.18, and 0.23), the present Nu_{avg} confirmed a satisfactory agreement with the experimental Nu_{avg} of Alhajaj et al [50]. At 0.18 (m^3/s) flow rate, Nu_{avg} represents a maximum deviation of 1.25%. The second validation appears in Figure 5, which illustrates thermal entropy generation/production (Sh) of HS with $\epsilon =$

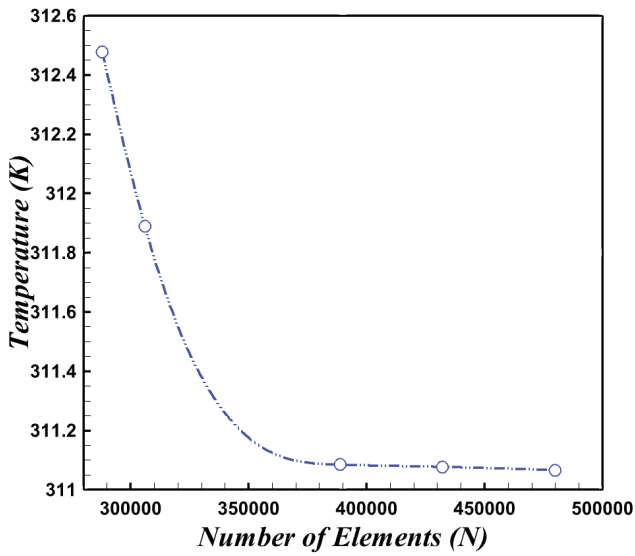


Figure 3. Grid independence test.

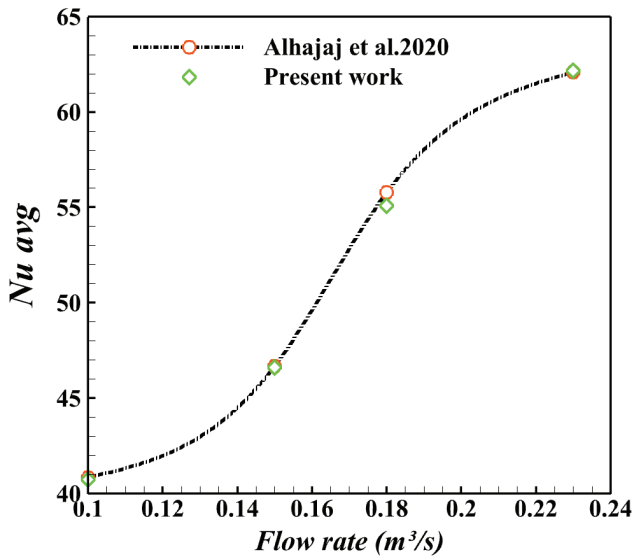


Figure 4. Comparison of Nu_{avg} of water in terms of different flow rates with the experimental results of Alhajaj et al. [50].

0.8 foam porosity at different Re . There is a good consistency between the outcome of the current study and what Ambreen et al. [47] found. The maximum error value observed at $Re = 600$ is 1.6%, which is acceptable for this study.

RESULTS AND DISCUSSION

Study and Selecting the Most Suitable Foam

The paper examines the effect of different mixing ratios of aluminum and copper in metallic foam on heat transfer

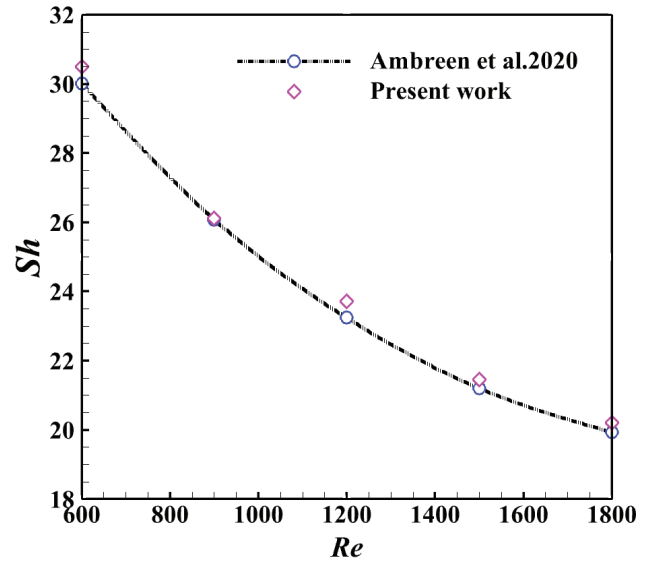


Figure 5. Validation of thermal entropy generation by the Eulerian model coupled with the Darcy-Brinkman-Forchheimer model of Ambreen et al. [47].

and entropy generation. Three other foams are studied, namely Al-Cu1 (80% Al and 20% Cu), Al-Cu2 (70% Al and 30% Cu), and Al-Cu3 (60% Al and 40% Cu). The goal is to find the optimal ratio that offers the best performance in CPU cooling while reducing entropy generation.

The variation of Nu_{avg} as a function of Re ($2600 \leq Re \leq 3800$) for different metal foams is shown in Figure 6 at $\phi = 0.1\%$. In agreement with the majority of previous studies [43, 48], Nu_{avg} increases as the flow acceleration. It is clear that Nu average of Al-Cu3 foam is always the highest, followed by Al-Cu2, then Al-Cu1, the aluminum foam gave

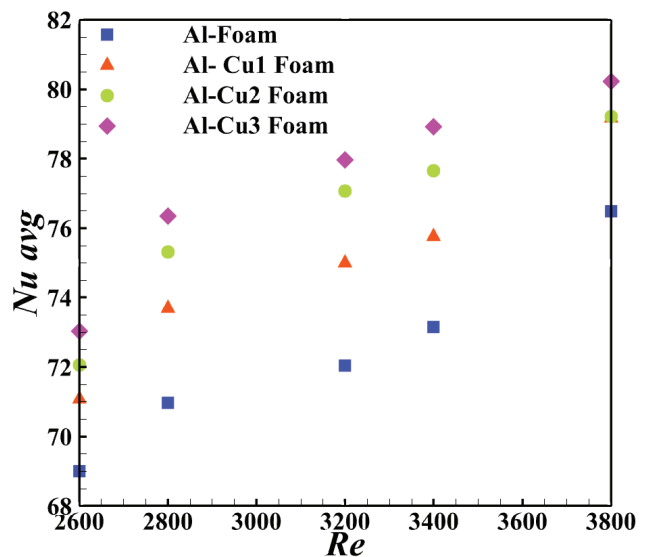


Figure 6. Average Nusselt number changes for various porous foams studied and Re number for $\phi = 0.1\%$.

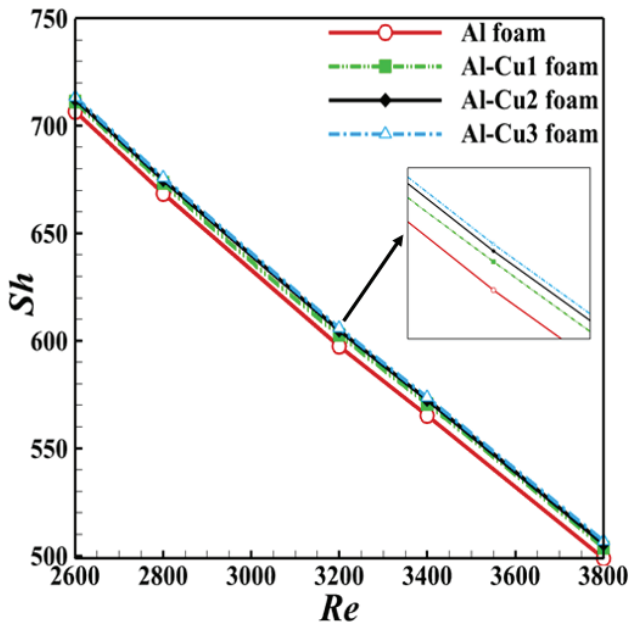


Figure 7. Thermal entropy generation as different Re number and metal foams for $\phi=0.1\%$.

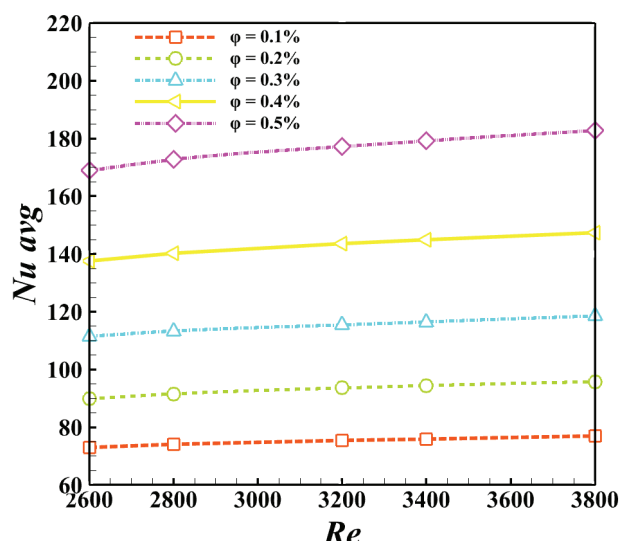
the lowest values, with an estimated deviation of 5.79% compared to Nu_{avg} of Al-Cu3 foam. This is the main reason for adding the percentages of copper in thoughtful foam, where copper has high thermal conductivity. Improved Nu_{avg} is more clear in Al-Cu3 foam containing 40% copper. This amount increased the thermal conductivity of the foam used in CPU cooling, as the heat exchange coefficient rises due to the forced convection of nf inside the foam, resulting in a lower convection/conduction ratio, increasing the Nusselt number. In $Re = 3800$, Nu_{avg} enhancement

is 4.84%. As the Cu ratio increases, Nu_{avg} improves. When Re rises from 2600 to 3800, Nu_{avg} reaches 9.86% and 9.76% for Al-Cu3 and Al foam, respectively.

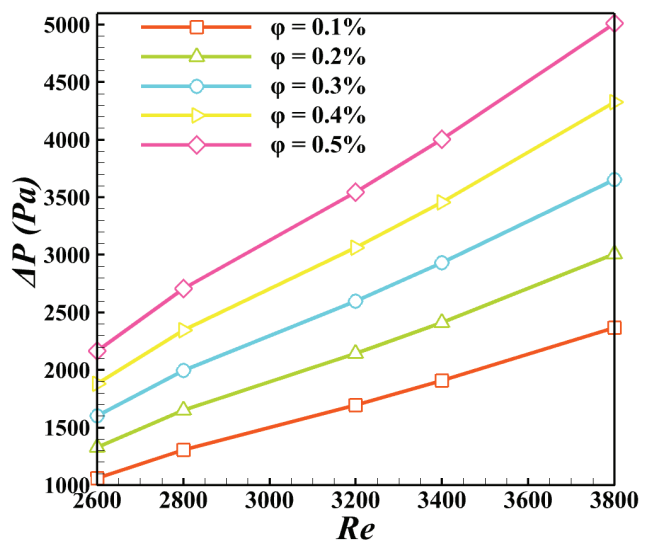
Figure 7 demonstrates the evolution of thermal entropy generation for different foams studied for $2800 \leq Re \leq 3800$ at np concentration ($\phi = 0.1\%$). Results show that there is an inverse ratio between S_h and Re , this is agreed in the previous paper [31]. As the Reynolds number increases, thermal entropy decreases. These results explain that the increasing percentage of copper in improved foam incited significant intermolecular disorder; in other words, more energy is dissipated from this system. This led to a higher entropy with Cu quantity. In addition, the rapid passage of nf through the porous medium accelerated the heat exchange by convection, causing a decrease in gradient temperature and a direct reduction in entropy. Large S_h values were obtained for Al-Cu3. In $Re = 2600$, the generating thermal entropy is 713.15. More clearly, adding copper to the metallic foam gave more force to the system, so entropy initially rose before it gradually declined, meaning that the amount of irreversible energy was more significant. Since Al-Cu3 gave better results regarding heat exchanger, this foam was considered in the rest of the study.

Hydrothermal Analysis

To understand the effects of np concentration ($\phi\%$) of $Fe_3O_4-H_2O$ on the thermal characteristics of the proposed HS, Nu_{avg} versus Re is indicated in Figure 8a for $Da = 10^{-1}$, $dn=10nm$. Nu_{avg} increased with the addition of np and flow rate, as agreed in previous studies [47, 50]. Nusselt number represents the ratio between convection and conduction. Acceleration of nf at different concentrations within metal foam leads to intense collisions with HS surfaces, racing the convection/conduction ratio. The addition of high-speed np reduces the thickness of the thermal boundary layer



a)



b)

Figure 8. Changes of a) Nu_{avg} , b) ΔP with Re at different nanoparticle concentrations $\phi\%$ for $Da=10^{-1}$, $dn=10$ nm.

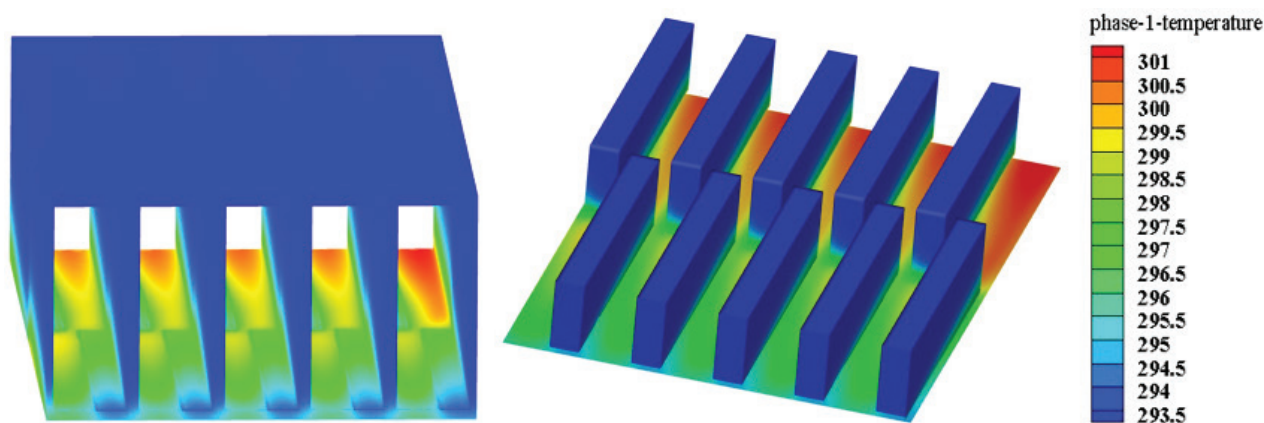


Figure 9. Effect of metal foam’s position on temperature variation (K).

on the heat sink’s bottom surface. All this improves heat exchange efficiency, which the Nusselts explain. When the volumetric concentration increased from 0.1% to 0.5%, for $2600 \leq Re \leq 3800$, Nu ranged from 56.71% to 57.91%. Figure 8b illustrates the evolution of pressure drops as a function of Re at different concentrations of np in water. High velocity and turbulence of Fe_3O_4 nf in HS channels lead to a gradual increase in pressure drop, which is evident when the percentage of nanoparticles is enhanced. For a Reynolds number raise from 2600 to 3800, the pressure drop is estimated at 55.34% and 56.82% for $\phi = 0.1\%$ and $\phi = 0.5\%$, respectively. The contrasting position of the porous medium and aggravation of collisions between nf and channel surfaces, especially with the presence of Al-Cu3 foam, resulted in this high energy loss.

Researchers are again trying to find the ideal position for the porous foam inside heat sinks to be effective in cooling. In this work, a different foam position was assumed as two opposing pieces in one cavity of HS. Figure 9 shows the temperature contour of HS at $Re = 2800$, $\phi = 0.2\%$, $Da = 10^{-1}$, and $dn = 10nm$. Temperature changes are at the lower basin surface and are more stable when porous media exist. The high conductivity of Al-Cu3 foam placed in opposite directions in HS channels enhanced surface exchange, and the high flow rate of $Fe_3O_4-H_2O$ nf improved heat transfer, allowing HS temperature to remain below 301 K. As shown, areas without porous foam have higher temperatures.

To clarify the effect of Al-Cu3 foam permeability on temperature distribution, Figure 10 plots temperature contours in different HS planes at $Re = 3200$, $\phi = 0.3\%$, $dn = 20nm$. Visually, isotherms are denser near the heated surface, which explains the heat transfer between HS and the CPU. In porous regions, the temperature is more steady, indicating that the porous medium was able to remove excess energy inside HS due to higher conductive heat transfer; this is more evident at a higher Darcy value. Moreover, In the $z = 22.5$ mm plane, which includes the opposite edges of the foam, the temperature lines near the bottom region are smooth and more ordered. The same behavior is obtained

at different permeabilities while increasing the length of temperature contours. To understand the mechanism of $Fe_3O_4-H_2O$ flow in the studied domain, Figure 11 shows the velocity profiles in the $z = 22.5$ mm plane (the middle of the domain) for different Da numbers at $Re = 3200$, $\phi = 0.3\%$, $dn = 20nm$. The velocity disturbance grows with decreasing Darcy’s number. In other words, low permeability prevents nf flow through pores, so it works as a block, forcing nf to rotate, which leads to vortices formation next to foam. In addition, at the top of HS, the liquid passage over the solid surface (metal foam) forms a boundary layer and leads to vortices forming At the highest Darcy value. The velocity lines are uniform and almost vortex-free due to the easy passage of nf; thus, heat transfer is enhanced. According to the results, it can be said that increasing pore permeability lowers the heated surface temperature and facilitates the passage of nf, resulting in an enhanced cooling process.

The Nusselt average number versus Reynolds number at different permeability of metal foam (Darcy number) is presented in Figure 12a. As can be seen, the heat transfer rate (Nu_{avg}) rises along with increases in Re and Da numbers. Similar results were found in previous studies [52-55]. Improved heat transfer while increasing Da is due to the high permeability of Al-Cu3 foam and thus easy access of nf to pores spaces. This is most evident in the high Reynolds number. Regardless of nf velocity, the low permeability of porous foam makes it difficult for the liquid to pass due to the small pore size and frequent friction between the nanoparticles and narrow pores. According to the results found, with all Reynolds values, raising Darcy’s from 10^{-4} to 10^{-1} improves Nu_{avg} by up to 23 %. The maximum value of Nu_{avg} is 95.816, obtained in $Re = 3800$ and $Da = 10^{-1}$. To reinforce the above results, Figure 12b illustrates the variation of ΔP as a function of Re at various Da. The increase in Da and Re values results in lower pressure drop values. Reduced pore permeability, or Da number, with high velocity, resulted in an undesired increase in friction due to the limited ability of nf to penetrate inside pores due to their small diameter, acting as an obstacle to nf flow, resulting

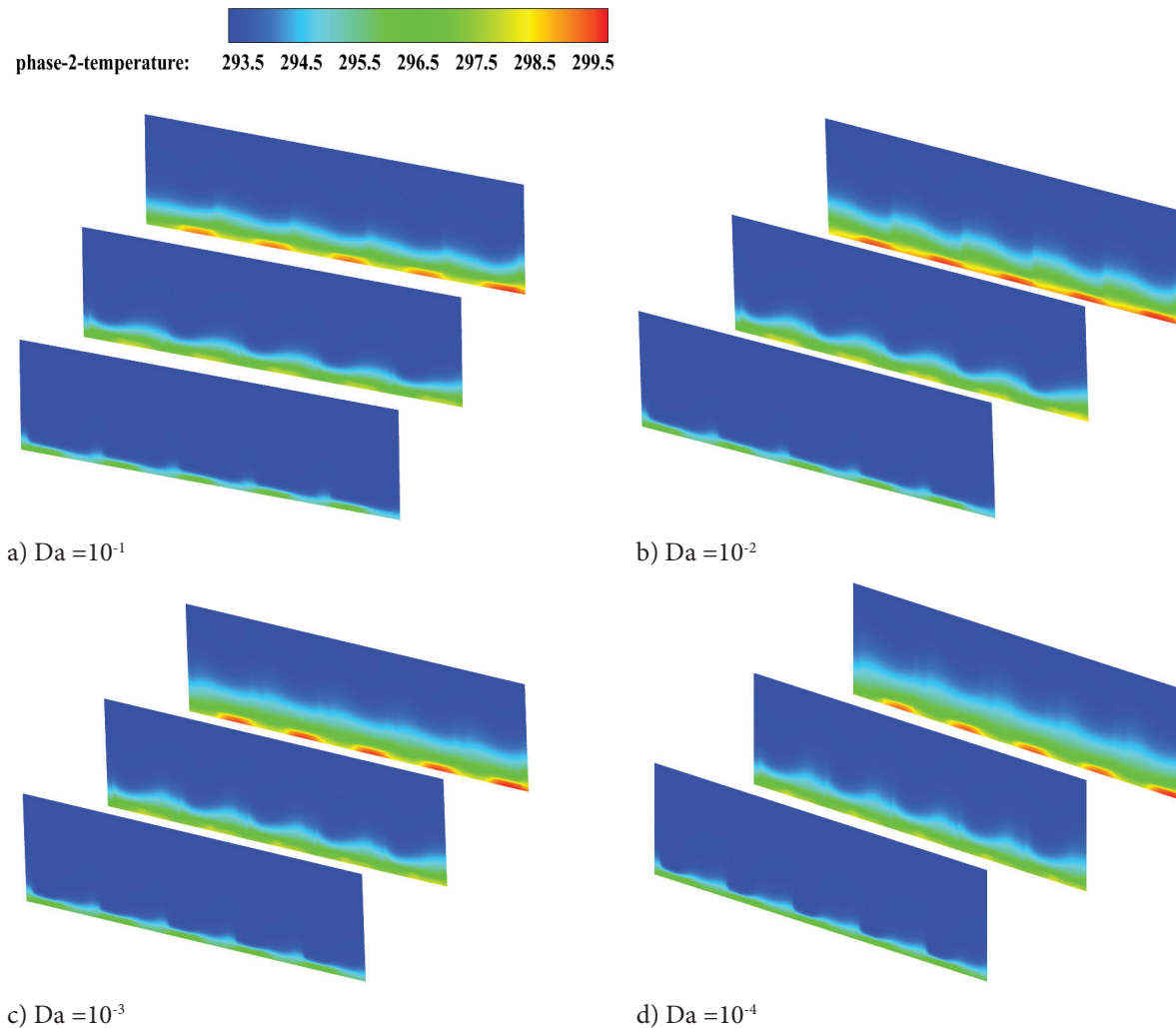


Figure 10. Heat sink temperature contours on the z-plane (5mm, 22.5mm, and 40mm) for various Da at Re = 3200, $\phi = 0.3\%$, $d_n = 20\text{nm}$.

in increased pressure drop values. For example, at $Da = 10^{-4}$ and $2800 \leq Re \leq 3800$, the amplification in ΔP is up to 55.15%. The increase in permeability facilitates the passage of nanofluid into pores and reduces friction, thus obtaining a lower pressure drop. The reduction in pressure drop is estimated at 87.53% for the same value of Re ($Re = 2600$) when Da changes from 10^{-4} to 10^{-1} .

Figure 13 depicts the evolution of Nu_{avg} with $\phi\%$ at different Da for $Re = 3200$, and $d_n = 20\text{nm}$. When np concentrations in base fluid rise, Nu_{avg} improves with the higher permeability of Al-Cu3 foam. It can be said that adding Fe_3O_4 np to water enhanced the cooled liquid's thermal conductivity. On the other hand, the thickness of the thermal boundary layer decreases due to forced convection of nf; with high permeability, the heat exchange between solid and porous medium is enhanced, rapidly reducing the temperature of HS. The maximum value of Nu_{avg} is 177.2 achieved for $Da = 10^{-1}$, $\phi = 0.5\%$. Improvement Nu_{avg} reaches 34.14% when Da is increased from 10^{-4} to 10^{-1} .

Figure 14 represents the relationship between heat transfer rate (Nu_{avg}) and diameter of nanoparticles (d_n) at various Re at $\phi = 0.1\%$ and $Da = 10^{-1}$. Results show a slight decrease in Nu average values with increasing np diameter and flow acceleration. This can be explained by the large size of the nanoparticle's diameter, which occupies more space, so the number of nanoparticles in the water decreases, inhibiting the movement and interaction between water molecules and Fe_3O_4 nanoparticles. This is why cooling efficiency is low. When the Re number increases, similar results are achieved.

Entropy Generation Analysis

Investigating entropy is one way of evaluating the heat exchange performance of engineering systems, especially heat sinks. Evaluation of entropy generation (entropy due to heat transfer S_h , entropy due to viscous dissipation S_p , and entropy due to the porous medium S_p) of Fe_3O_4 - H_2O

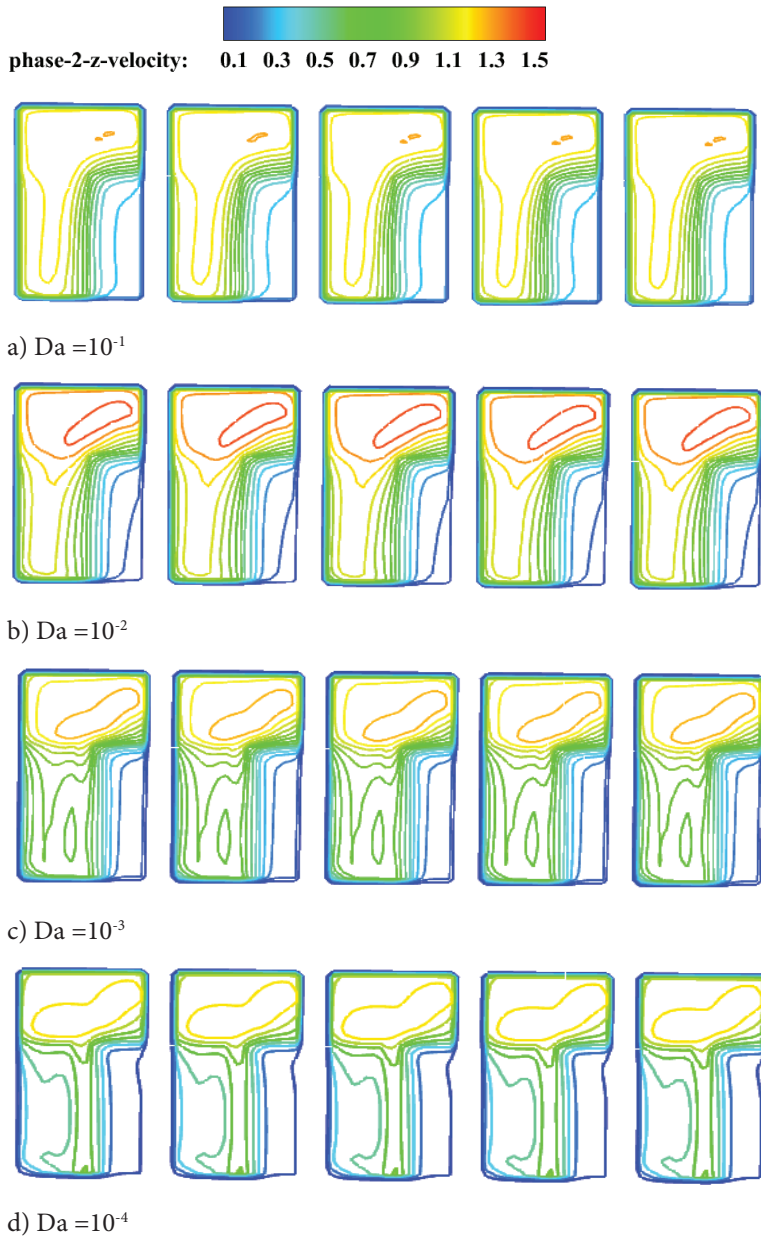


Figure 11. Velocity counters in the middle of HS at $Re=3200$, $\varphi=0.3\%$, $dn=20nm$ for different Da .

nf in Al-Cu3 foam with various parameters (Re , Da , $\varphi\%$) are investigated in this section.

Figure 15 presents the a) S_h , b) S_p , c) S_f , and d) S_g , in different Re and $\varphi\%$ for $Da=10^{-1}$ and $dn=20nm$. In agreement with general trends [31], the thermal and global entropy generation shows the inverse dependence on Re caused by a lower temperature gradient directly affected by forced convection. Moreover, adding np leads to a significant decrease in entropy generation values due to the penetration of nf with high thermal conductivity into pores, stabilizing the surface temperature. Based on equation (22), temperature gradient strongly affects thermal entropy production; a more homogeneous medium means a lower entropy value. As Figure 15a shows, when $Re=2600$, the thermal entropy

generation decreased by 47.58%, but the loss is more remarkable at $Re=3800$, evaluated by 81.18%.

Figure 15b and 15c demonstrate the variation of entropy production due to porous media and viscous entropy generation as a function of Re with various concentrations of np , respectively. The S_p and S_f are directly proportional to Re and $\varphi\%$. The porous panels placed next to the walls of HS increase the velocity slope of nf . In contrast, the velocity gradient is significant, increasing the entropy generation value due to friction and porous foam. Moreover, the viscosity of nf rises with the increase of $\varphi\%$ in water, resulting in higher friction force. This is due to the internal force between the layers of liquid, which is at its maximum when in contact with a solid surface. By fixing Re in 3200,

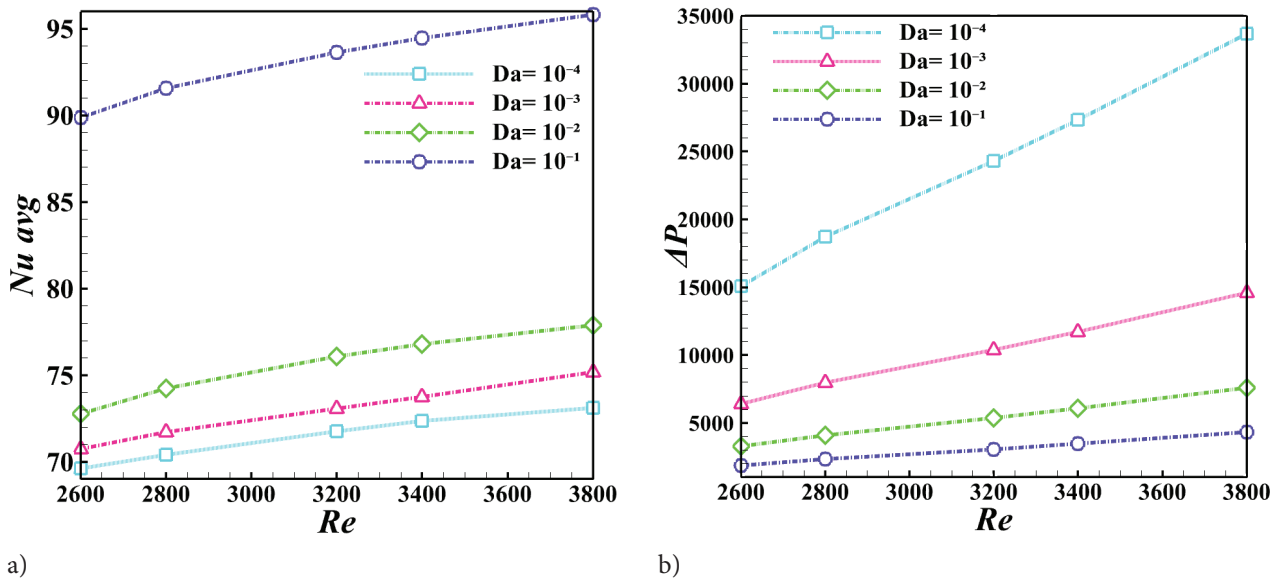


Figure 12. Variation of Nu_{avg} and pressure drop in Re at different Da for $\phi = 0.2\%$, $dn=10nm$.

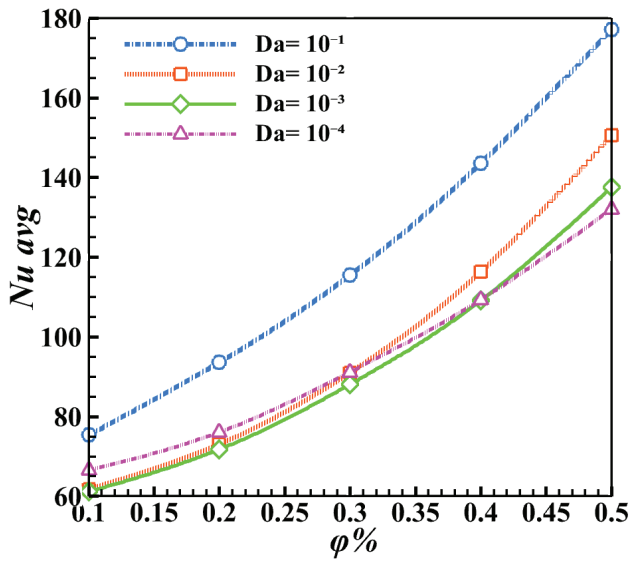


Figure 13. Nu_{avg} as a function of nanoparticles concentrations $\phi\%$ for various Da number at $Re=3200$, $dn =20nm$.

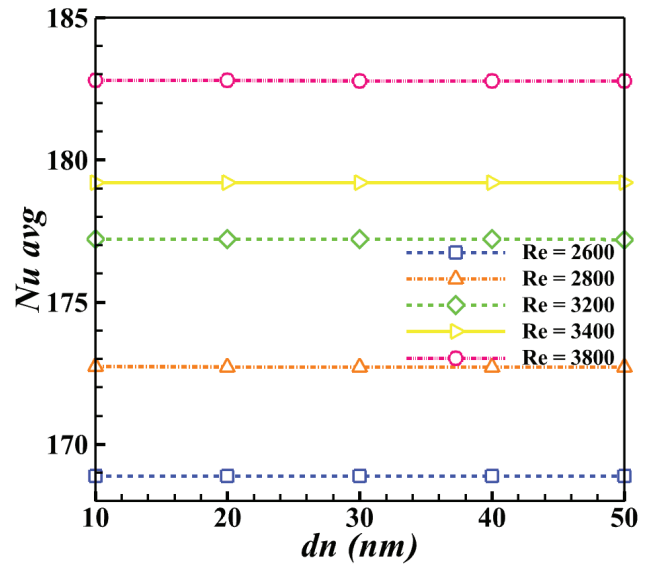


Figure 14. Changes of Nu_{avg} with dn at different Re for $\phi = 0.5\%$, $Da=10^{-1}$.

S_p grows by 45.8% and S_f by 77.3% when np concentration rises from 0.1% to 0.5%. Concerning the total entropy depicted in Figure 15d, according to its equation (25), it is the sum of thermal entropy generation, viscous, and due to porous medium. Considering each other's values, changes in total entropy generation are mainly affected by changes in thermal entropy generation during their dominance, and the rest is slightly influenced.

The influence of Darcy's number or, more precisely, the effect of Al-Cu3 foam permeability and np concentrations on the entropy generation is demonstrated at constant Re ($Re=3200$) and constant diameter of np ($dn = 20nm$) in

Figure 16. According to the results obtained, S_h grows rapidly with Da values and np concentration. On the other side, S_f gives the highest values at the smallest Darcy because the friction reaches the maximum due to the obstruction of nf flow in the narrow pores. As the pores expand due to the increase in Da , the friction reduces, and the transit of liquid becomes easy, resulting in a lower temperature gradient in the porous part, reducing the thermal entropy and increasing the heat exchanger process through forced convection. Furthermore, for S_p , it was shown that their value increases significantly at $Da=10^{-4}$, with the highest value being 48.17, estimated at $\phi=0.5\%$, while not exceeding 0.72

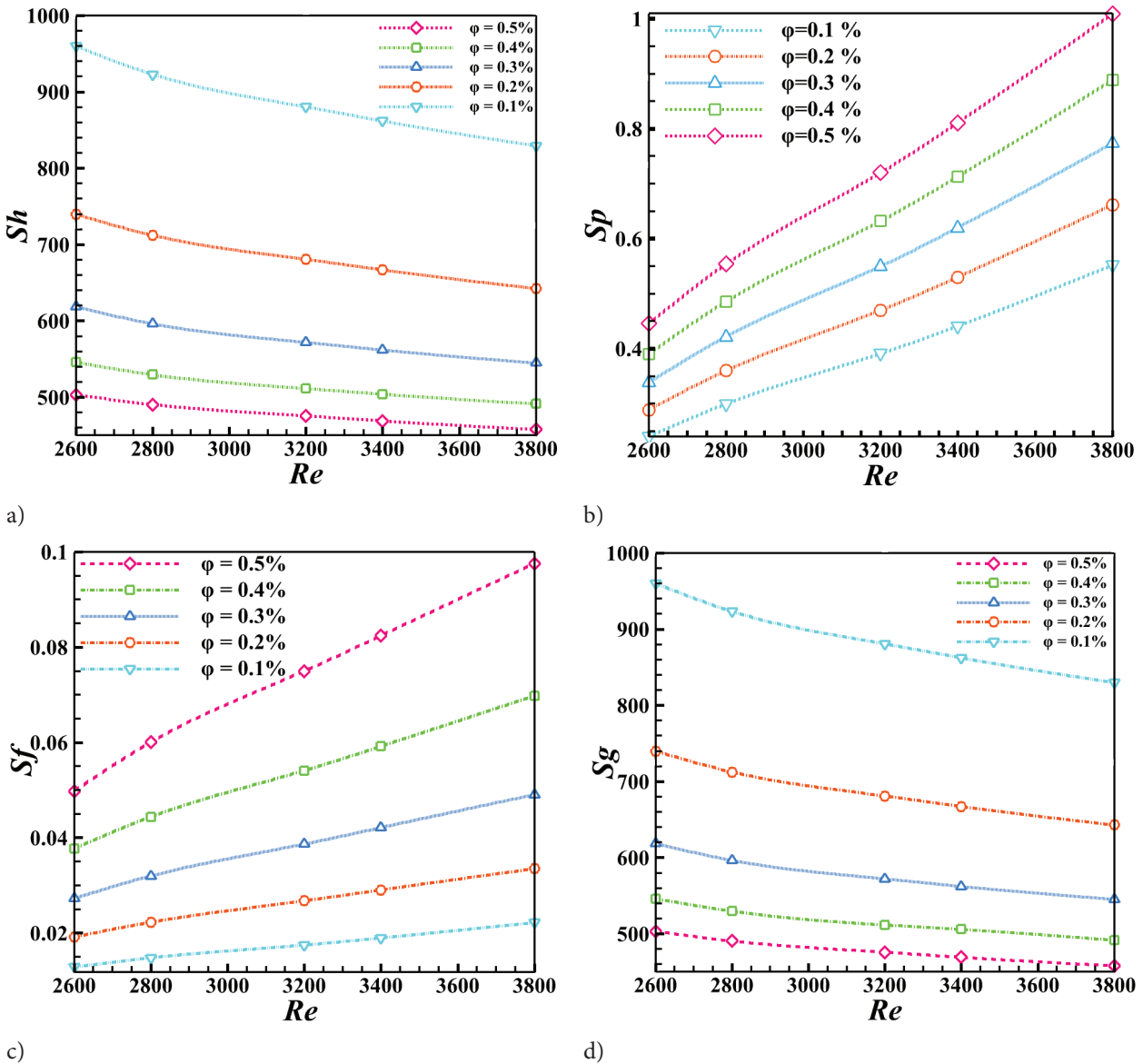


Figure 15. Effects of Re on entropy generation with different $\phi\%$ at $Da=10^{-1}$, $dn=20nm$.

when Darcy is 10^{-1} . As seen in Figure 16b, entropy values generated by porous media converge with high permeability. Since thermal entropy increases with rising $\phi\%$ and Da , the total entropy displays the same behavior due to its dominance over the total. In Figure 16d, for a value of $Da=10^{-4}$, at low concentrations of np , a disparity in entropy values is present, where the value of total entropy increases due to the increase of S_p values, which has a significant impact on the randomness of the system. With higher concentrations and high permeability, this effect gradually disappears. Generally, it can be argued that the factor strongly influencing entropy production is temperature gradient and permeability of pores. In other words, the low temperature of exchange surfaces leads to a weak thermal entropy, which means that the medium is less disordered, which is explained by the total entropy.

The outcomes of thermal entropy and entropy due to the porous media in metal foam HS versus flow acceleration and Da are indicated in Figure 17. In all Darcy values, the thermal entropy reduces with increased nf flux. In contrast, the resulting entropy of the porous medium rises with increased Re values. As discussed, enhancing $Fe_3O_4-H_2O$ nf velocity within reinforced metal foam accelerates heat exchange, decreasing the temperature gradient and lowering thermal entropy values. Thermal entropy values are almost identical when Darcy goes from $Da=10^{-2}$ to $Da=10^{-1}$. From these results, it can be said that pore permeability has a slight effect compared to high nf velocity. As shown in Figure 17b, S_p raises with Re . The increase is perceptible at lower Da values due to enhanced velocity, especially on the z -axis parallel to nf track.

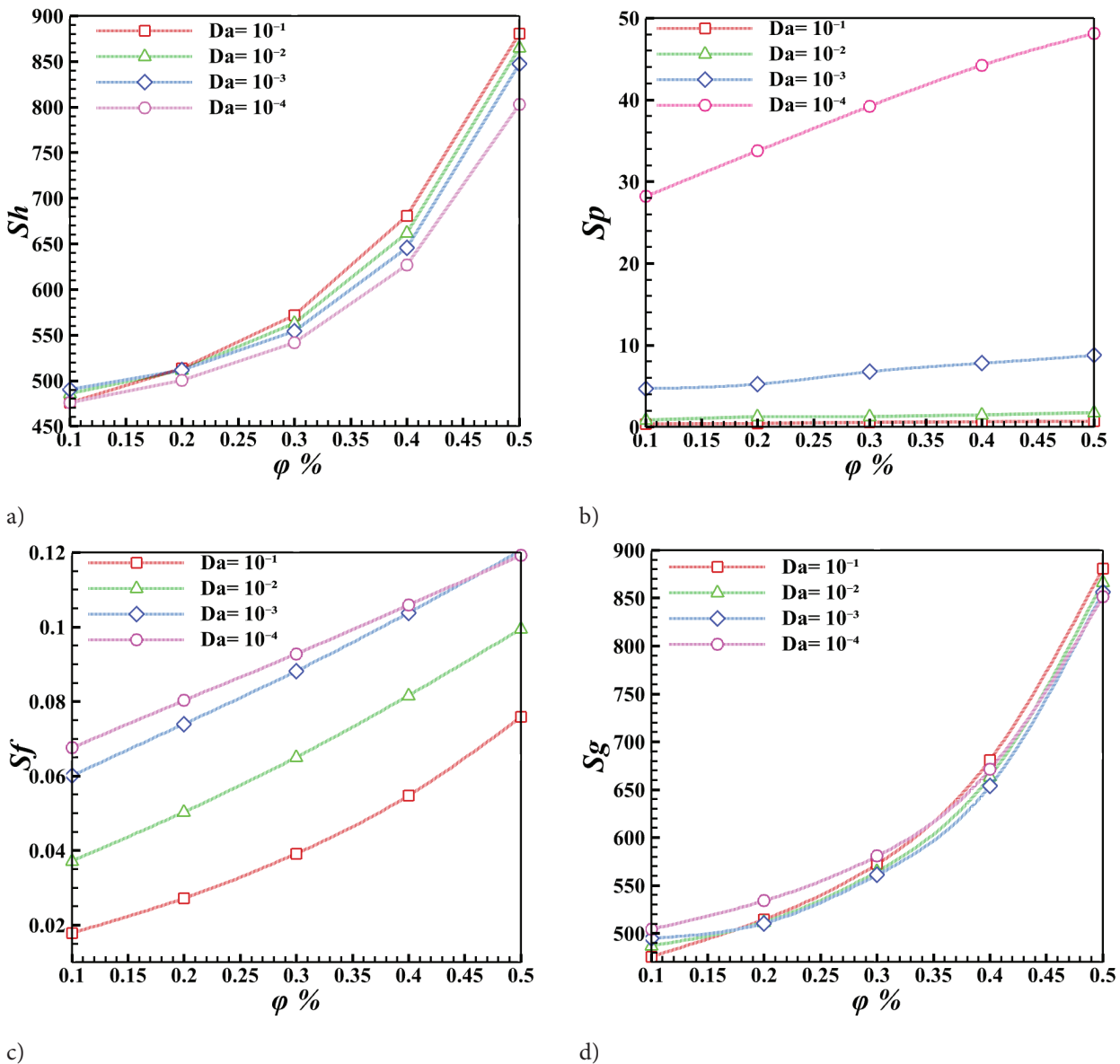


Figure 16. Changes of a) S_h , b) S_p , c) S_f , and d) S_g with ϕ % at different Da for $Re=3200$, $dn=20$ nm.

The dependency of friction factor on flow velocity for different np concentrations is displayed in Figure 18. According to equation (21), the friction factor is influenced by various parameters such as pressure drop, flow velocity, channel size, and nf properties. Fe_3O_4 np in water induces slight friction between HS walls' basic and adjacent fluid layers. Hence, enhancing the concentrations of nanoparticles with higher Reynolds numbers increases the friction coefficient. Similar observation were reported by Chan et al.[56] in their investigation. As previously explained in Figure 8, pressure drop grows with increased coolant velocity and np concentrations due to the high viscosity of Fe_3O_4 - H_2O nf, which has a direct influence on the growth of the friction factor. At a constant value of Re , the friction

factor rises to 49.6% when the concentration is changed from 0.1% to 0.5%.

Figure 19 exposes the HS performance evaluation criteria changes at different Darcy and Reynolds numbers for $\phi=0.2\%$, $dn=20$ nm. Results display enhancement in PEC as pore permeability and flow velocity are raised. Noticeably, there is an important variation in HS performance when Darcy reaches the maximum, while the PEC values are almost constant when Da moves from 10^{-4} to 10^{-2} . Although the pressure drop of nf within pores increases (shown in Figure 12b), heat transfer is more dominant, improving the performance evaluation criteria. The enhancement is up to 56%.

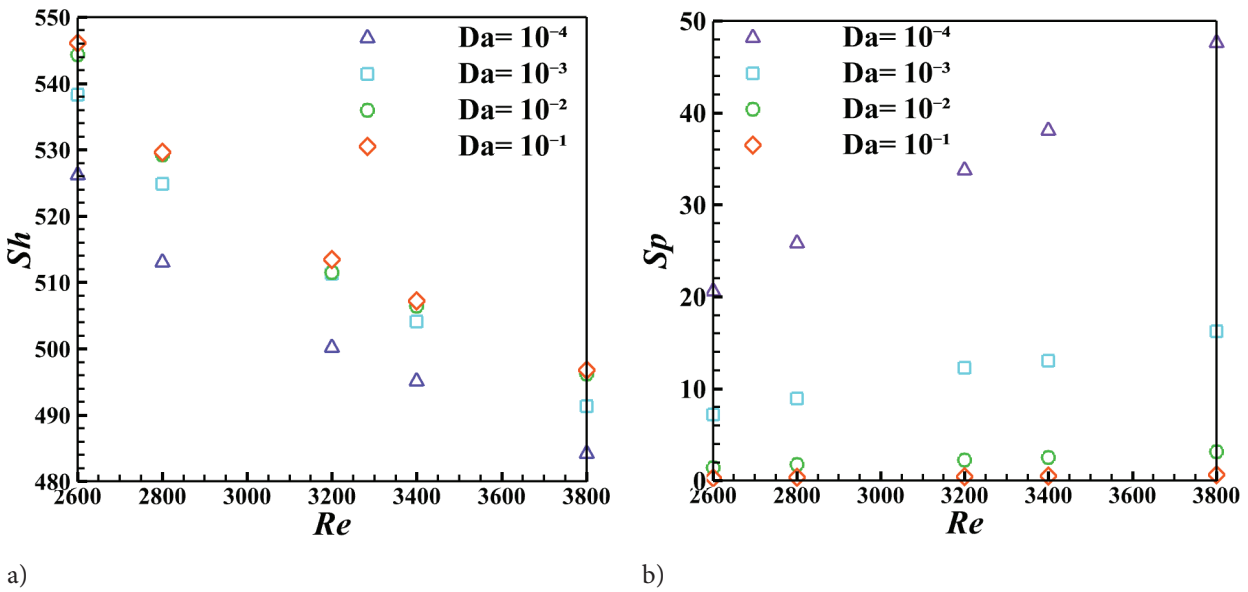


Figure 17. Variations of S_h , b) S_p as a function of Re at different Da numbers.

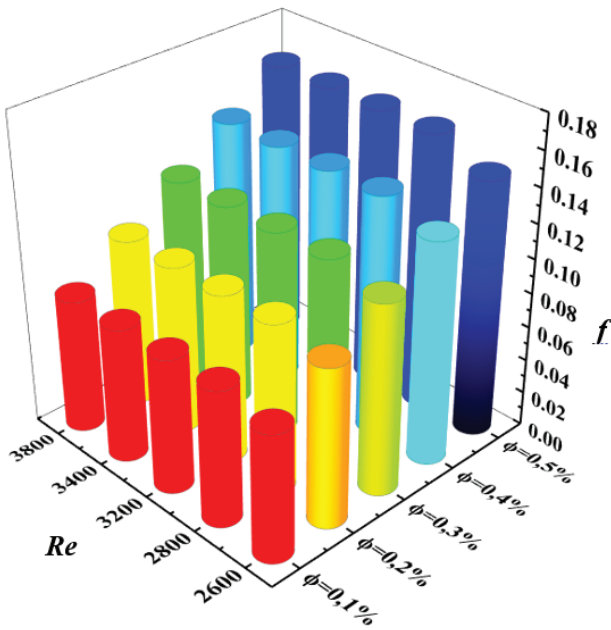


Figure 18. Friction factor as a function of Re at various concentrations of nanoparticles.

CONCLUSION

To obtain an effective metal foam for cooling the Core i9 processor, this paper compared several metal foams in terms of aluminum and copper mixture ratios. The optimal foam was selected and installed in a new opposite shape inside the proposed heat sink. The finite volume method (FVM) simulated the computational domain under turbulent and forced convection conditions. To increase the study’s accuracy, a two-phase Eulerian approach was used

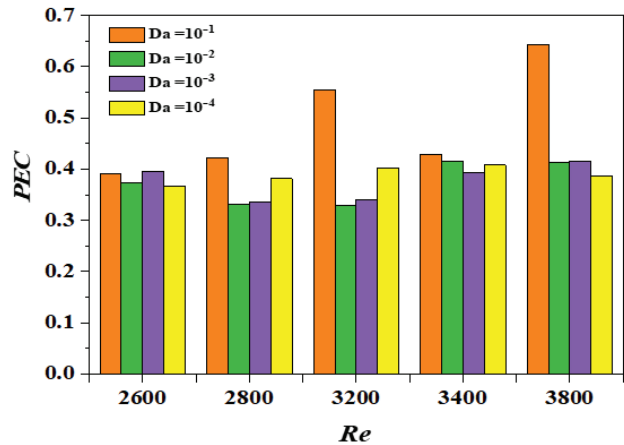


Figure 19. Performance evaluation criteria of HS with Da and Re numbers.

to predict the behavior of Fe_3O_4 nf in foam. The study investigated the influence of flow velocity, np diameter and concentration, and pore permeability on heat transfer and entropy generation. The results were presented as Nu average, pressure drop, temperature and velocity contours, and entropy generation. The main results obtained can be summarized as follows:

- 1 Al-Cu3 foam, which contains 60% aluminum and 40% copper, improves heat transfer by up to 5.79% with a constant porosity ($\epsilon = 0.8$).
- 2 The addition of Fe_3O_4 nanoparticles to the base fluid at different concentrations leads to an enhancement of Nu_{avg} from 56.71% to 57.91, also accompanied by an increase in pressure drop from 55.34% to 56.82% when ϕ rises from 0.1 to 0.5, respectively.

- 3 Increasing n_f flow rate while improving pore permeability leads to a 23% enhancement in Nu_{avg} at $\phi=0.2\%$, $d_n=10nm$.
- 4 The placement of metal foam proposed in this study can reduce the thermal entropy production by 47.58% and 81.18% for Re values of 2600 and 3800, respectively.
- 5 Performance evaluation criteria PEC improves to 56% when the pore permeability and flow velocity are raised.
- 6 Using Al-Cu₃ foam can effectively maintain the temperature of electronic components within the safe limit. Finally, field experiments could be carried out to determine how the position of porous media and its composition affect cooling efficiency in electronic components. Other nanofluids or hybrid nanofluids can be tested as coolants.

NOMENCLATURE

A	Area (m ²)
Al	Aluminum foam
C _p	Specific heat (J/kg.K)
Cu	Copper foam
Da	Darcy number
d _n	Nanoparticles diameter (nm)
f	Friction factor
H	Height (mm)
h	Convective heat transfer coefficient (W/m ² K)
h	Height of Al-Cu ₃ foam (mm)
HS	Heat sink
K	Permeability (m ²)
k	Heat conductivity (W/m.K)
L	Length (mm)
l	Length of Al-Cu ₃ foam (mm)
MCHS	Micro Channel Heat Sink
MHD	Magneto-hydrodynamic
Nu	Nusselt number
Nu_{avg}	Average Nusselt number
P	Pressure (Pa)
ΔP	Pressure drop (Pa)
PCM	Phase change material
PEC	Performance evaluation criteria
q''	Heat flux (W/ m ²)
S _h	Thermal entropy generation
T	Temperature (K)
t	Length of space between two foams (mm)
W	Width (mm)
w	Width of Al-Cu ₃ foam (mm)

Greek Symbols

μ	Viscosity (kg/m.s)
ρ	Density (kg/m ³)
ϕ	Volume fraction of nanoparticles (%)
ε	Porosity

Subscripts

avg	Average
in	Inlet

l	Liquid phase
n_f	Nanofluid
n_p	Nanoparticle
p	Solid phase
out	Outlet

AUTHORSHIP CONTRIBUTIONS

Authors equally contributed to this work.

DATA AVAILABILITY STATEMENT

The authors confirm that the data that supports the findings of this study are available within the article. Raw data that support the finding of this study are available from the corresponding author, upon reasonable request.

CONFLICT OF INTEREST

The author declared no potential conflicts of interest with respect to the research, authorship, and/or publication of this article.

ETHICS

There are no ethical issues with the publication of this manuscript.

REFERENCES

- [1] Sundar LS, Sharma KV, Singh MK, Sousa ACM. Hybrid nanofluids preparation, thermal properties, heat transfer and friction factor - A review. *Renew Sustain Energy Rev* 2017;68:108. [\[CrossRef\]](#)
- [2] Habibishandiz M, Saghir MZ. A critical review of heat transfer enhancement methods in the presence of porous media, nanofluids, and microorganisms. *Therm Sci Eng Prog* 2021;30:101267. [\[CrossRef\]](#)
- [3] Tang Z, Qi C, Tian Z, Chen L. Thermal management of electronic components based on new wave bio-inspired structures and nanofluids. *Int Commun Heat Mass Transf* 2021;131:105840. [\[CrossRef\]](#)
- [4] Zhao N, Guo L, Qi C, Chen T, Cui X. Experimental study on thermo-hydraulic performance of nanofluids in CPU heat sink with rectangular grooves and cylindrical bugles based on exergy efficiency. *Energy Convers Manag* 2018;181:076. [\[CrossRef\]](#)
- [5] Kesavan D, Kumar RS, Marimuthu P. Heat transfer performance of air-cooled pin-fin heatsinks: a review. *J Therm Anal Calorim* 2023;148:11691. [\[CrossRef\]](#)
- [6] Bin Kwak D, Kwak HP, Noh JH, Yook SJ. Optimization of the radial heat sink with a concentric cylinder and triangular fins installed on a circular base. *J Mech Sci Technol* 2018;32:1252. [\[CrossRef\]](#)
- [7] Wu J, et al. Thermal performance improvement of a heat-sink using metal foams for better energy storage systems. *J Energy Storage* 2022;60:106663. [\[CrossRef\]](#)

- [8] Ebrahimi-Moghadam A, Moghadam AJ. Optimal design of geometrical parameters and flow characteristics for Al₂O₃/water nanofluid inside corrugated heat exchangers by using entropy generation minimization and genetic algorithm methods. *Appl Therm Eng* 2018;149:068. [\[CrossRef\]](#)
- [9] He Z, Yan Y, Zhang L. Thermal-hydraulic investigation on micro heat sinks with ribbed pin-fin arrays and single heating input: parametrical study. *J Therm Anal Calorim* 2022;147:10977. [\[CrossRef\]](#)
- [10] Jeng TM, Tzeng SC, Tseng CW, Chang CH. Effects of passage divider and packed brass beads on heat transfer characteristic of the pin-fin heat sink by water cooling. *Heat Mass Transf und Stoffuebertragung* 2020;56:02725. [\[CrossRef\]](#)
- [11] Khan U, et al. Radiative mixed convective flow induced by hybrid nanofluid over a porous vertical cylinder in a porous media with irregular heat sink/source. *Case Stud Therm Eng* 2021;30:101711. [\[CrossRef\]](#)
- [12] Ahmadian-Elmi MBS, Hajmohammadi MR, Nourazar SS, Vafia K. Investigating the effect of the presence of a pulsating heat pipe on the geometrical parameters of the microchannel heat sink. *Numer Heat Transf Part A Appl* 2023;2188330. [\[CrossRef\]](#)
- [13] Yao Z, et al. Numerical assessment of the impacts of non-Newtonian nanofluid and hydrophobic surfaces on conjugate heat transfer and irreversibility in a silicon microchannel heat-sink. *J Taiwan Inst Chem Eng* 2022;142:104642. [\[CrossRef\]](#)
- [14] K. C, M. P. C, A. C, M. Numerical study on the performance of Al₂O₃/water nanofluids as a coolant in the fin channel heat sink for an electronic device cooling. *Mater Today Proc* 2023;337.
- [15] Hashemi-Tilehnoee M, Palomo del Barrio E. Magneto laminar mixed convection and entropy generation analyses of an impinging slot jet of Al₂O₃-water and Novec-649. *Therm Sci Eng Prog* 2022;36:101524. [\[CrossRef\]](#)
- [16] Wang Y, et al. A three-dimensional flow of an Oldroyd-B liquid with magnetic field and radiation effects: An application of thermophoretic particle deposition. *Int Commun Heat Mass Transf* 2022;134:106007. [\[CrossRef\]](#)
- [17] Hashemi-Tilehnoee M, del Barrio EP, Seyyedi SM. Magneto-turbulent natural convection and entropy generation analyses in liquid sodium-filled cavity partially heated and cooled from sidewalls with circular blocks. *Int Commun Heat Mass Transf* 2022;134:106053. [\[CrossRef\]](#)
- [18] Ramzan M, Ali F, Akkurt N, Saeed A, Kumam P, Galal AM. Computational assessment of Carreau ternary hybrid nanofluid influenced by MHD flow for entropy generation. *J Magn Magn Mater* 2022;567:170353. [\[CrossRef\]](#)
- [19] Izadi A, Siavashi M, Rasam H, Xiong Q. MHD enhanced nanofluid mediated heat transfer in porous metal for CPU cooling. *Appl Therm Eng* 2019;168:114843. [\[CrossRef\]](#)
- [20] Iqbal J, Abbasi FM, Alkinidri M, Alahmadi H. Heat and mass transfer analysis for MHD bioconvection peristaltic motion of Powell-Eyring nanofluid with variable thermal characteristics. *Case Stud Therm Eng* 2022;43:102692. [\[CrossRef\]](#)
- [21] Cheng J, Xu H, Tang Z, Zhou P. Multi-objective optimization of manifold microchannel heat sink with corrugated bottom impacted by nanofluid jet. *Int J Heat Mass Transf* 2023;201:123634. [\[CrossRef\]](#)
- [22] Kushawaha D, Yadav S, Singh DK. Magnetic field effect on double-diffusion with magnetic and non-magnetic nanofluids. *Int J Mech Sci* 2020;191:106085. [\[CrossRef\]](#)
- [23] Yanala VSR, Reddy DB, Goud BS, Nalivela NR. Impact of porosity on two-dimensional unsteady MHD boundary layer heat and mass transfer stagnation point flow with radiation and viscous dissipation. *Numer Heat Transf Part A Appl* 2023;2198739.
- [24] Baghsaz S, Rezanejad S, Moghimi M. Numerical investigation of transient natural convection and entropy generation analysis in a porous cavity filled with nanofluid considering nanoparticles sedimentation. *J Mol Liq* 2019;279:117. [\[CrossRef\]](#)
- [25] Chai L, Wang L. Thermal-hydraulic performance of interrupted microchannel heat sinks with different rib geometries in transverse microchambers. *Int J Therm Sci* 2018;127:029. [\[CrossRef\]](#)
- [26] Hemmat Esfe M. Viscosity analysis of MWCNT (25%)-ZnO(75%)/10W40 hybrid nanofluid; toward a new look at finding efficient nanofluid for heat transfer goals. *Arab J Sci Eng* 2021;46:05091. [\[CrossRef\]](#)
- [27] Saravanan V, Umesh CK. Numerical comparison for thermo-hydraulic performance of pin fin heat sink with microchannel pin fin heat sink. *Sadhana Acad Proc Eng Sci* 2018;43:0875. [\[CrossRef\]](#)
- [28] Arafa AAM, Ahmed SE, Allan MM. Peristaltic flow of non-homogeneous nanofluids through variable porosity and heat generating porous media with viscous dissipation: Entropy analyses. *Case Stud Therm Eng* 2022;32:101882. [\[CrossRef\]](#)
- [29] Maghrabie HM, et al. Microchannel heat sinks with nanofluids for cooling electronic components: Performance enhancement, challenges, and limitations. *Therm Sci Eng Prog* 2022;37:101608. [\[CrossRef\]](#)
- [30] Deshmukh VRR. Experimental and numerical analysis of effect of combined drop-shape pin fins and plate fins type heat sink under natural convection. *Numer Heat Transf Part A Appl* 2023;2195128. [\[CrossRef\]](#)
- [31] Yang M, et al. A performance evaluation method based on the Pareto frontier for enhanced microchannel heat sinks. *Appl Therm Eng* 2022;212:118550. [\[CrossRef\]](#)

- [32] Buonomo B, di Pasqua A, Manca O, Nappo S, Nardini S. Entropy generation analysis of laminar forced convection with nanofluids at pore length scale in porous structures with Kelvin cells. *Int Commun Heat Mass Transf* 2022;132:105883. [\[CrossRef\]](#)
- [33] Bahiraei M, Mazaheri N, Daneshyar MR, Mwesigye A. Two-phase simulation of irreversibilities for Ag-water nanofluid flow inside an elliptical pin-fin heat sink: Entropy generation and exergy considerations. *Powder Technol* 2022;409:117723. [\[CrossRef\]](#)
- [34] Yang M, Li MT, Hua YC, Wang W, Cao BY. Experimental study on single-phase hybrid micro-channel cooling using HFE-7100 for liquid-cooled chips. *Int J Heat Mass Transf* 2020;160:120230. [\[CrossRef\]](#)
- [35] Chang YC. Simulation analysis of heat transfer performance of heat sink with reduced material design. *Adv Mech Eng* 2020;12:1687814020921300. [\[CrossRef\]](#)
- [36] Jawad M, Shah Z, Khan A, Islam S, Ullah H. Three-dimensional magnetohydrodynamic nanofluid thin-film flow with heat and mass transfer over an inclined porous rotating disk. *Adv Mech Eng* 2019;11:1687814019869757. [\[CrossRef\]](#)
- [37] Boudraa B, Bessaïh R. Numerical investigation of heat transfer around a hot block subject to a cross-flow and an extended jet hole using ternary hybrid nanofluids. *J Mech Eng Sci* 2022;236:09544062211049872. [\[CrossRef\]](#)
- [38] Adegbola AA, Olajide G, Mudashiru LO, Adeaga OA. Numerical investigation of enhanced oil recovery with steam injection. *Int J Manag IT Eng* 2018;8.
- [39] Farrukh BM, Chen GM, Tso CP. Viscous dissipation effect on CuO-water nanofluid-cooled microchannel heat sinks. *Case Stud Therm Eng* 2020;26:101159. [\[CrossRef\]](#)
- [40] Reddy NK, Swamy HAK, Sankar M, Jang B. MHD convective flow of Ag-TiO₂ hybrid nanofluid in an inclined porous annulus with internal heat generation. *Case Stud Therm Eng* 2022;42:102719. [\[CrossRef\]](#)
- [41] Zhang B, Zhu J, Gao L. Topology optimization design of nanofluid-cooled microchannel heat sink with temperature-dependent fluid properties. *Appl Therm Eng* 2020;176:115354. [\[CrossRef\]](#)
- [42] Yang M, Cao BY. Multi-objective optimization of a hybrid microchannel heat sink combining manifold concept with secondary channels. *Appl Therm Eng* 2020;181:115592. [\[CrossRef\]](#)
- [43] Krishnan SRA, Sivan S, Midhun VC, Behera SR. Experimental and numerical investigation of solid-solid phase change material assisted heat sink with integrated heat pipe for electronic cooling. *J Energy Storage* 2022;59:106494. [\[CrossRef\]](#)
- [44] Mirshekar A, Goodarzi MR, Mohebbi-Kalhari D, Shafiei Mayam MH. Experimental study of heat transfer enhancement using metal foam partially filled with phase change material in a heat sink. *J Energy Storage* 2022;60:106496. [\[CrossRef\]](#)
- [45] Rehman T, Ambreen T, Niyas H, Kanti P, Ali HM, Park CW. Experimental investigation on the performance of RT-44HC-nickel foam-based heat sinks for thermal management of electronic gadgets. *Int J Heat Mass Transf* 2022;188:122591. [\[CrossRef\]](#)
- [46] Bayomy AM, Saghir MZ, Yousefi T. Electronic cooling using water flow in aluminum metal foam heat sink: Experimental and numerical approach. *Int J Therm Sci* 2016;109:007. [\[CrossRef\]](#)
- [47] Ambreen T, Saleem A, Park CW. Analysis of hydro-thermal and entropy generation characteristics of nanofluid in an aluminium foam heat sink by employing Darcy-Forchheimer-Brinkman model coupled with multiphase Eulerian model. *Appl Therm Eng* 2020;173:115231. [\[CrossRef\]](#)
- [48] Qi C, Li K, Li C, Shang B, Yan Y. Experimental study on thermal efficiency improvement using nanofluids in heat sink with heated circular cylinder. *Int Commun Heat Mass Transf* 2020;114:104589. [\[CrossRef\]](#)
- [49] Zargartalebi M, Azaiez J. Heat transfer analysis of nanofluid based microchannel heat sink. *Int J Heat Mass Transf* 2018;127:152. [\[CrossRef\]](#)
- [50] Alhajaj Z, Bayomy AM, Saghir MZ, Rahman MM. Flow of nanofluid and hybrid fluid in porous channels: Experimental and numerical approach. *Int J Thermofluids* 2020;1-2:100016. [\[CrossRef\]](#)
- [51] ANSYS. *Fluent Theory Guide*. Canonsburg, PA: ANSYS Inc.; 2014.
- [52] Kandavel TK, Vignesh J, Vijak D. Effect of porous on thermal behaviour of sintered P/M iron material. *J Therm Eng* 2023;10:1621-1631. [\[CrossRef\]](#)
- [53] Aruna J, Niranjana H. Effects of electric field, MHD micropolar hybrid nanofluid flow with mixed convection and thermal radiation across a flat surface. *J Therm Eng* 2023;10:1607-1620. [\[CrossRef\]](#)
- [54] Garvandha M, Gajjala N, Narla V, Kumar D. Thermodynamic entropy of a magnetized nanofluid flow over an inclined stretching cylindrical surface. *J Therm Eng* 2023;10:1253-1265. [\[CrossRef\]](#)
- [55] Nath JM, Paul A, Das TK. Heat transfer characteristics of magnetohydrodynamic Casson stratified hybrid nanofluid flow past a porous stretching cylinder. *J Therm Eng* 2023;10:1137-1148. [\[CrossRef\]](#)
- [56] Shah AH, Memon LA, Luhur MR, Jamali QB, Bhangwar SH, Rajput UA. Performance and fluid flow analysis of double pipe heat exchanger using Al₂O₃-nanofluid. *J Therm Eng* 2023;10:1120-1136. [\[CrossRef\]](#)